Receding Horizon Pseudo-Spectral Control for Energy Maximization of a $1/25^{th}$ Scale Hinge-Barge Wave Energy Converter

Francesco Paparella[1] and John V. Ringwood[2]
Centre for Ocean Energy Research (COER)
Maynooth University, Co. Kildare, Ireland
E-mail: [1]francesco.paparella.2014@mumail.ie , [2]john.ringwood@nuim.ie

***Abstract*—This paper addresses the real-time optimal control of a $1/25^{th}$ scale three-body hinge-barge wave energy device. The objective of the control is to maximize the power extracted by the device under given constraints on the maximum displacements, velocities and control forces. An optimal pseudo-spectral control based on the Half-Range Chebyshev-Fourier basis functions is presented. HRCF basis functions are well suited for the approximation of non-periodic signals, allowing the representation of both the transient and steady-state response of the device. A reduced equivalent dynamic model of the device, which is computationally more advantageous than a full dynamic model, is obtained for the optimal control problem formulation. Results show that pseudo-spectral control outperforms a simple control strategy based on the optimal constant passive damping for both monochromatic and polychromatic waves.**

***Index Terms*—Multi-body wave energy converter, receding horizon, energy maximization, pseudo-spectral control, 1/25 th scale model.**

I. Introduction

A multibody hinge-barge Wave Energy Converter (WEC) is composed of different rectangular bodies interconnected by joints. The relative motion between each pair of bodies drive a Power Take Off (PTO) system which is used to extract energy from the device. The objective of the control is to maximize the power extracted from the device under given constraints on the maximum displacements, velocities and control forces. In [1], an optimal Pseudo-Spectral (PS) control of a $1/25^{th}$ scale three-body hinge-barge device based on Fourier-series basis functions is considered for a finite time horizon. PS methods are a subset of the class of techniques used for the discretisation of integral and partial differential equations known as mean weighted residuals [2], [3]. Apart from providing a solution for the dynamics of a multi-body system, PS methods can also be used to efficiently solve an optimal control problem for the device [4].

Fourier-series basis functions can only represent the steady-state response of the device. Therefore, with Fourier-series basis functions, the motion of the device is considered to be periodic and the transient effects of the dynamics of the device are neglected. Therefore, the optimal control with PS methods based on Fourier basis functions cannot be applied for the real-time control of the WEC, but provides an useful framework for the evaluation of the achievable power absorption under both active and passive control.

This paper addresses the real-time optimal control of a $1/25^{th}$ scale three-body hinge-barge device. For the optimal control of WECs, the Model Predictive Control (MPC) strategy has been adopted in [5]. In [6], a broad overview on MPC-like controllers for WECs is presented. In this paper, an optimal PS control based on the Half-Range Chebyshev-Fourier (HRCF) basis functions [7] is presented. HRCF basis functions are well suited for the approximation of non-periodic signals, allowing the representation of both the transient and steady-state response of the device. HRCF functions represents a Fourier extension for nonperiodic signals and, therefore, are especially suited for the wave energy field, since wave elevation and fluidstructure interaction forces are all well described using Fourier analysis. In [8], a receding horizon PS control with HRCF basis functions is applied to a flap device.

The remainder of the paper is organized as follows: in Section II, a full dynamic model of a three-body hinge-barge device is derived while, in Section III, a reduced equivalent dynamic model of the device is obtained for the optimal control problem formulation. In Section IV, a receding horizon optimal PS control based on the HRCF basis functions is presented while, in Section V, a convex cost function for PS control with HRCF basis functions is proposed. In Section VI, results on PS control with HRCF basis functions applied to a $1/25^{th}$ scale three-body hinge-barge device are shown for both monochromatic and polychromatic waves. Finally, overall conclusions are drawn in Section VII.

II. Full Dynamic Model of a Three-body Hinge-barge Device

This section briefly describes the full dynamic model of a three-body hinge-barge device in the frequency domain originally derived in [1]. In Figure 1, the device is represented together with the global frame X_g, Z_g, while a body frame is assigned to each body composing the device. The number of degrees of freedom of the device is $n = 4$: the heave displacement z_2 of body 2, the pitch angle θ_2 of body 2 and the relative pitch angles $\theta_{rel,1}$ and $\theta_{rel,2}$ of bodies 1 and 3, respectively. Therefore, the vector of independent velocities of the device is:

$$\mathbf{v}_s = [\dot{z}^b_{i,b_2}\ \dot{\theta}_2\ \dot{\theta}_{rel,1}\ \dot{\theta}_{rel,2}]^T \tag{1}$$

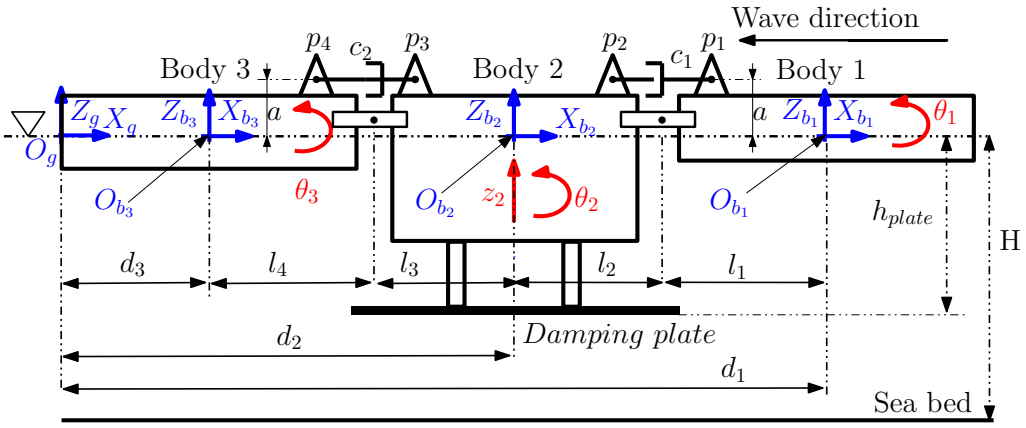

Fig. 1. Three-body hinge-barge device, where $X_g Z_g$ represents the global frame, and a local frame is assigned to each body composing the device.

Note that, in Figure 1, the incoming wave travels from the right to the left, as body 1 is the forward barge of the WEC. The PTO is made of two dashpots placed above the hinges and connecting body 2 to body 1 and 3, as shown in Figure 1. The control forces are represented by PTO torques acting on the relative pitch motion between body 2 and body 1 and 3. The number of control forces is $n_c = 2$. The full dynamic model of the device in the frequency domain is given as follows:

$$\begin{aligned}(-\omega^2 \left(\mathbf{M}_s + \mathbf{M}_{a,s}(\omega)\right) + j\omega \left(\mathbf{B}_{rad,s}(\omega) + \mathbf{B}_{visc,s}\right) + .. \\ \mathbf{G}_s)\hat{\mathbf{X}}(\omega) = \mathbf{H}_{ex}(\omega)\eta + \mathbf{F}_{pto}\mathbf{U}\end{aligned} \tag{2}$$

where $\hat{\mathbf{X}} \in \mathbb{R}^{n\times 1}$ is the position vector, $\mathbf{U} \in \mathbb{R}^{n_c\times 1}$ is the control force vector, $\mathbf{F}_{pto}$ is the configuration matrix of the PTO, $\mathbf{M}_s$ is the inertia matrix, $\mathbf{B}_{visc,s}$ is the viscous damping matrix, $\mathbf{G}_s$ is the hydrostatic stiffness, $\mathbf{M}_{a,s}$ is the added mass, $\mathbf{B}_{rad,s}$ is the radiation damping and $\mathbf{H}_{ex}$ is the transfer function between the excitation force vector and the wave elevation. Note that the viscous damping force vector acting on the WEC in (2), is considered to be linearly proportional to the velocity vector, with a proportionality matrix $\mathbf{B}_{visc,s}$. The use of a viscous damping force vector, which is linearly proportional to the velocity vector, allows to represent the dynamics of the WEC with a linear full dynamic model. The computational effort required to PS methods to solve the optimal control problem is greatly reduced by using a linear full dynamic model, instead of a nonlinear full dynamic model, for the description of the dynamics of the WEC. Moreover, the viscous damping matrix $\mathbf{B}_{visc,s}$ of a linear full dynamic model of the WEC can be easily tuned to fit the wave-tank tests carried out on the WEC, as presented in [9].

III. Equivalent Reduced Dynamic Model for Control Formulation

The full dynamic model in (2) is described in terms of the motion of the degrees of freedom of the device. An equivalent reduced dynamic model which is described only in terms of the relative pitch rotations between the barges can be obtained [10], [11]. The full dynamic model of the device in (2) can be rewritten in frequency domain as follows:

$$(\mathbf{R} + j\omega\mathbf{C})\hat{\mathbf{V}} = \mathbf{H}_{ex}\eta + \mathbf{F}_{pto}\mathbf{U} \tag{3}$$

where:

$$\hat{\mathbf{V}} = \begin{bmatrix}\dot{Z}^b_{i,b_2} & \dot{\Theta}_2 & \dot{\Theta}_{rel,1} & \dot{\Theta}_{rel,2}\end{bmatrix}^T \tag{4}$$

$$\mathbf{R} = \begin{bmatrix}\mathbf{R}_{11} & \mathbf{R}_{12} \\ \mathbf{R}_{21} & \mathbf{R}_{22}\end{bmatrix} = \mathbf{B}_{rad,s}(\omega) + \mathbf{B}_{visc,s} \tag{5}$$

$$\mathbf{C} = \begin{bmatrix}\mathbf{C}_{11} & \mathbf{C}_{12} \\ \mathbf{C}_{21} & \mathbf{C}_{22}\end{bmatrix} = \mathbf{M}_s + \mathbf{M}_{a,s}(\omega) - \frac{\mathbf{G}_s}{\omega^2} \tag{6}$$

$$\mathbf{H}_{ex} = \begin{bmatrix}\mathbf{H}_{ex,1} & \mathbf{H}_{ex,2}\end{bmatrix}^T \tag{7}$$

$$\mathbf{F}_{pto} = \begin{bmatrix}\mathbf{0}_2 & \mathbf{I}_2\end{bmatrix}^T \tag{8}$$

The dependency of the variables and matrixes in (3)-(7) from ω is dropped in order to simplify the notation. Then, equation (3) can be written as a system of two matrix equations:

$$\begin{bmatrix}\dot{Z}^b_{i,b_2} \\ \dot{\Theta}_2\end{bmatrix} = \mathbf{Z}_f^{-1}\left(\mathbf{H}_{ex,1}\eta - \frac{\mathbf{G}_s}{\omega^2}\mathbf{T}\begin{bmatrix}\dot{\Theta}_{rel,1} \\ \dot{\Theta}_{rel,2}\end{bmatrix}\right) \tag{9}$$

$$\begin{aligned}(\mathbf{R}_{22} + j\omega\mathbf{C}_{22})\begin{bmatrix}\dot{\Theta}_{rel,1} \\ \dot{\Theta}_{rel,2}\end{bmatrix} = \mathbf{H}_{ex,2}\eta + \mathbf{U} - .. \\ (\mathbf{R}_{21} + j\omega\mathbf{C}_{21})\begin{bmatrix}\dot{Z}^b_{i,b_2} \\ \dot{\Theta}_2\end{bmatrix}\end{aligned} \tag{10}$$

where $\mathbf{Z}_f = \mathbf{R}_{11} + j\omega\mathbf{C}_{11}$ and $\mathbf{T} = \mathbf{R}_{12} + j\omega\mathbf{C}_{12}$. Substituting equation (9) into (10) yields the following equivalent reduced model for the relative pitch rotations:

$$\mathbf{A}_{eq}\begin{bmatrix}\dot{\Theta}_{rel,1} \\ \dot{\Theta}_{rel,2}\end{bmatrix} = \mathbf{H}_{eq}\eta + \mathbf{U} \tag{11}$$

where:

$$\mathbf{A}_{eq} = \mathbf{R}_{22} - \mathbf{R}_{21}\mathbf{Z}_f^{-1}\mathbf{T} + j\omega\left(\mathbf{C}_{22} - \mathbf{C}_{21}\mathbf{Z}_f^{-1}T\right) \quad (12)$$

$$\mathbf{H}_{eq} = \mathbf{H}_{ex,2} - j\omega\mathbf{C}_{2,1}\mathbf{Z}_f^{-1}\mathbf{H}_{ex,1} - \mathbf{R}_{2,1}\mathbf{Z}_f^{-1}\mathbf{H}_{ex,1} \quad (13)$$

As shown in (11), the equivalent reduced model is described in terms of the relative pitch rotations which are the modes that are used to extract energy from the device. Therefore, the equivalent reduced dynamic model is particularly suitable for the formulation of the control problem since it involves a smaller number of variables than the full dynamic model. However, with the equivalent reduced dynamic model, the information on the heave and pitch rotation of the central barge is lost. Therefore, the equivalent reduced dynamic model represents a less comprehensive description of the motion of the device than the fully dynamic model, but it reduces the computational effort required to the controller.

In order to express the dynamic model in (11) in the time domain, the equivalent added mass at infinity and inertia matrix need to be computed. If $\mathbf{A}_{eq}$ in (12) is written as follows:

$$\mathbf{A}_{eq} = \mathbf{R}_{eq} + j\omega\left(\mathbf{M}_{eq,in} + \mathbf{M}_{eq,a} - \frac{\mathbf{G}_{eq}}{\omega^2}\right) \quad (14)$$

where $\mathbf{R}_{eq}$ is the equivalent radiation damping matrix, $\mathbf{M}_{eq,in}$ is the equivalent inertia matrix, $\mathbf{M}_{eq,a}$ is the equivalent added mass matrix and $\mathbf{G}_{eq}$ is the equivalent stiffness matrix. Therefore, the equivalent added mass at infinity and the inertia matrix are given as follows:

$$\lim_{\omega\to\infty}\frac{\mathrm{Im}\{\mathbf{A}_{eq}\}}{\omega} = \mathbf{M}_{eq,in} + \mathbf{M}_{eq,\mathrm{inf}} \quad (15)$$

where $\mathbf{M}_{eq,\mathrm{inf}}$ is the equivalent added mass at infinity. The equivalent stiffness matrix is given as follows:

$$\lim_{\omega\to 0}\omega\,\mathrm{Im}\{\mathbf{A}_{eq}\} = -\mathbf{K}_{eq} \quad (16)$$

Finally, the equivalent reduced model expressed in the time domain is given as:

$$\dot{\mathbf{q}}_{eq} = \mathbf{v}_{eq} \quad (17)$$

$$\mathbf{M}_{eq,tot}\dot{\mathbf{v}}_{eq} + \mathbf{B}_{eq,visc}\mathbf{v}_{eq} + \mathbf{G}_{eq}\mathbf{q}_{eq} + .. \int_0^t \mathbf{k}_{eq,rad}(t-\tau)\mathbf{v}_{eq}, d\tau = \mathbf{f}_{eq,wave} + \mathbf{u} \quad (18)$$

where $\mathbf{q}_{eq} \in \mathbb{R}^{n\times 1}$ is the position vector, $\mathbf{v}_{eq} \in \mathbb{R}^{n\times 1}$ is the velocity vector, $\mathbf{u} \in \mathbb{R}^{n_c\times 1}$ is the control force vector, $\mathbf{M}_{eq,tot} = \mathbf{M}_{eq,in} + \mathbf{M}_{eq,\mathrm{inf}}$, $\mathbf{B}_{eq,visc}$ is the equivalent viscous damping matrix, $\mathbf{k}_{eq,rad}$ is the kernel function matrix of the equivalent radiation forces and $\mathbf{f}_{eq,wave}$ is the equivalent wave excitation force vector.

IV. Receding Horizon Pseudospectral Control

This section describes the direct transcription of the optimal control problem for a 3-body hinge-barge device. The vector of control variables is considered to be $\mathbf{u} = [\tau_1\ \tau_2]^T$, where τ_1 is the torque applied by the PTO connecting body 2 and 1, while τ_2 is the torque applied by the PTO connecting body 2 and 3. The objective of the optimal control problem is to compute the trajectories of the PTO torques and velocities of the bodies of device in order to maximize the energy absorbed by the device. The average power absorbed by the PTOs, over the time interval $[0, T]$, is given as:

$$J = \frac{1}{T}\int_{t_0}^{t_0+T}\mathbf{v}_{eq}^T\mathbf{u}dt \quad (19)$$

For simplicity, the time interval $[t_0, t_0 + T]$ is mapped into the time interval $[-1, 1]$ by using the following affine transformation $g : t \to \tau$:

$$\tau = g(t) = \frac{2}{T}(t - t_0) - 1 \quad (20)$$

where $t \in [t_0, t_0 + T]$ and $\tau \in [-1, 1]$. Using the affine transformation in (20), equations (17) and (18) can be written as:

$$\dot{\mathbf{Q}}_{eq} = \frac{T}{2}\mathbf{V}_{eq} \quad (21)$$

$$\dot{\mathbf{V}}_{eq} = \frac{T}{2}\mathbf{M}_{eq,tot}^{-1}\Big(-\mathbf{B}_{eq,visc}\mathbf{V}_{eq} - \mathbf{G}_{eq}\mathbf{Q}_{eq} - .. \int_{g^{-1}(0)}^{\tau}\mathbf{K}_{eq,rad}(\tau - s + g(0)^{-1})\mathbf{V}_{eq}ds + \mathbf{F}_{eq,wave} + \mathbf{U}\Big) \quad (22)$$

where $\mathbf{Q}_{eq} = \mathbf{q}_{eq} \circ g$ is the scaled position vector, $\mathbf{V}_{eq} = \mathbf{v}_{eq} \circ g$ is the scaled velocity vector, $\mathbf{K}_{eq,rad} = \mathbf{k}_{eq,rad} \circ g$ is the scaled kernel function matrix of the radiation forces, $\mathbf{F}_{eq,wave} = \mathbf{f}_{eq,wave} \circ g$ and $\mathbf{U} = \mathbf{u} \circ g$ is the scaled control force vector. The average power absorbed by the PTOs, over the time interval $[-1, 1]$, is given as:

$$J = \frac{1}{2}\int_{-1}^{1}\mathbf{V}_{eq}^T\mathbf{U}d\tau \quad (23)$$

The optimal control problem consists of computing the vector of PTO torques that maximize the cost function in (23), subject to the equations of motion (21)-(22). Additional constraints on the applied torques, relative pitch displacements and velocities can be considered in the optimal control formulation.

The positions, velocities and control forces can be approximated as a combination HRCF basis functions as follows [8]:

$$Q_{eq,i}(\tau) \approx Q_{eq}^M(\tau) = \sum_{k=0}^{M} x_{i,k}^{q,c}T_k^h\left(cos\frac{\pi}{2}\tau\right) + \sum_{k=0}^{M-1} x_{i,k}^{q,s}U_k^h\left(cos\frac{\pi}{2}\tau\right)sin\frac{\pi}{2}\tau = \mathbf{\Phi}(\tau)^T\hat{\mathbf{x}}_i^q \quad (24)$$

$$V_{eq,i}(\tau) \approx V_{eq}^{M}(\tau) = \sum_{k=0}^{M} x_{i,k}^{v,c} T_k^h \left(cos\frac{\pi}{2}\tau\right) + \sum_{k=0}^{M-1} x_{i,k}^{v,s} U_k^h \left(cos\frac{\pi}{2}\tau\right) sin\frac{\pi}{2}\tau = \mathbf{\Phi}(\tau)^T \hat{\mathbf{x}}_i^v \tag{25}$$

$$U_i(\tau) \approx U_i^{M}(\tau) = \sum_{k=0}^{M} u_{p,k}^{c} T_k^h \left(cos\frac{\pi}{2}\tau\right) + \sum_{k=0}^{M-1} u_{p,k}^{s} U_k^h \left(cos\frac{\pi}{2}\tau\right) sin\frac{\pi}{2}\tau = \mathbf{\Phi}(\tau)^T \hat{\mathbf{u}}_p \tag{26}$$

where $i = 1, .., n_c$, $p = 1, .., n_c$ and M is the order of expansion of the approximation. The vector of the coefficients $\hat{\mathbf{x}}_i^q$, $\hat{\mathbf{x}}_i^v$ and $\hat{\mathbf{u}}_p$ of the approximated components of the position, velocity and control vectors, are given as follows:

$$\hat{\mathbf{x}}_i^q = \begin{bmatrix} x_{i,0}^{q,c} \; x_{i,1}^{q,c} \; .. \; x_{i,M-2}^{q,s} \; x_{i,M-1}^{q,s} \end{bmatrix}^T \tag{27}$$

$$\hat{\mathbf{x}}_i^v = \begin{bmatrix} x_{i,0}^{v,c} \; x_{i,1}^{v,c} \; .. \; x_{i,M-2}^{v,s} \; x_{i,M-1}^{v,s} \end{bmatrix}^T \tag{28}$$

$$\hat{\mathbf{u}}_p = \begin{bmatrix} u_{p,0}^{c} \; u_{p,1}^{c} \; .. \; u_{p,M-2}^{s} \; u_{p,M-1}^{s} \end{bmatrix}^T \tag{29}$$

while the basis function vector $\mathbf{\Phi}(t)$ is given as follows:

$$\mathbf{\Phi}(\tau) = \Big[T_0^h \left(cos\frac{\pi}{2}\tau\right) \;\; T_1^h \left(cos\frac{\pi}{2}\tau\right) \;\; .. \; T_M^h \left(cos\frac{\pi}{2}\tau\right) \; U_0^h \left(cos\frac{\pi}{2}\tau\right) sin\frac{\pi}{2}\tau \;\; .. \;\; U_{M-1}^h \left(cos\frac{\pi}{2}\tau\right) sin\frac{\pi}{2}\tau \Big]^T \tag{30}$$

By substituting the approximated velocities and control torques defined in (25) and (26), respectively, into the expression for the absorbed power defined in (23), the approximated average absorbed power is given as:

$$\begin{aligned} J^M &= \frac{1}{2}\int_{-1}^{1} \mathbf{\Phi}(\tau)^T \mathbf{X}^V \mathbf{U}^T \mathbf{\Phi}(\tau) d\tau \\ &= \frac{1}{2}(\; \hat{\mathbf{u}}_1^T \hat{\mathbf{x}}_1^v + \hat{\mathbf{u}}_2^T \hat{\mathbf{x}}_2^v) \\ &= \frac{1}{4}\mathbf{x}^T \mathbf{H} \mathbf{x} \end{aligned} \tag{31}$$

where:

$$\mathbf{X}^V = [\; \hat{\mathbf{x}}_1^v, .., \hat{\mathbf{x}}_{n_c}^v] \tag{32}$$

$$\mathbf{U} = [\; \hat{\mathbf{u}}_1, .., \hat{\mathbf{u}}_{n_c}] \tag{33}$$

$$\mathbf{x} = [\; \hat{\mathbf{x}}^{q,T} \; \hat{\mathbf{x}}^{v,T} \; \hat{\mathbf{u}}^T]^T \tag{34}$$

$$\mathbf{H} = \begin{bmatrix} \mathbf{0}_{N,N} & \mathbf{0}_{N,N} & \mathbf{0}_{N,N} \\ \mathbf{0}_{N,N} & \mathbf{0}_{N,N} & \mathbf{H}_1 \\ \mathbf{0}_{N,N} & \mathbf{H}_2 & \mathbf{I}_N \end{bmatrix} \tag{35}$$

$$\mathbf{H}_1 = \begin{bmatrix} \mathbf{I}_{2M+1} & \mathbf{0}_{2M+1} \\ \mathbf{0}_{2M+1} & \mathbf{I}_{2M+1} \end{bmatrix} \tag{36}$$

$$\mathbf{H}_2 = \mathbf{H}_1^T \tag{37}$$

with $N = n_c \times 2M + 1$. The derivatives of the ith components of the position and velocity vector are, respectively,

$$\dot{Q}_{eq,i}^{M}(\tau) = \dot{\mathbf{\Phi}}(\tau)^T \hat{\mathbf{x}}_i^q = \mathbf{\Phi}(\tau)^T \mathbf{D} \hat{\mathbf{x}}_i^q \tag{38}$$

$$\dot{V}_{eq,i}^{M}(\tau) = \dot{\mathbf{\Phi}}(\tau)^T \hat{\mathbf{x}}_i^v = \mathbf{\Phi}(\tau)^T \mathbf{D} \hat{\mathbf{x}}_i^v \tag{39}$$

where $\mathbf{D} \in \mathbb{R}^{2M+1 \times 2M+1}$ is a block diagonal matrix given as follows [12]:

$$\mathbf{D} = \frac{\pi}{2}\begin{bmatrix} \mathbf{0} & \mathbf{H}_1 \\ \mathbf{H}_2 & \mathbf{0} \end{bmatrix} \tag{40}$$

Substituting the approximated states (24), (25) and their time derivatives (38), (39) into the equations of motion (21)-(22), yields the following equations of motion in residual form:

$$r_i^q(\tau) = \mathbf{\Phi}(\tau)\mathbf{D}\hat{\mathbf{x}}_i^q - \mathbf{\Phi}(\tau)\hat{\mathbf{x}}_i^v \tag{41}$$

$$\begin{aligned} r_i^v(\tau) = &\sum_{p=1}^{n_c} \frac{2}{T} M_{eq,tot_{i,p}} \mathbf{\Phi}(\tau)\mathbf{D}\hat{\mathbf{x}}_p^v + .. \\ &\sum_{p=1}^{n_c} B_{eq,visc_{i,p}} \mathbf{\Phi}(\tau)\hat{\mathbf{x}}_p^v + \sum_{p=1}^{n_c} G_{eq_{i,p}} \mathbf{\Phi}(\tau)\hat{\mathbf{x}}_p^q + .. \\ &\sum_{p=1}^{n_c} \int_{g(0)^{-1}}^{\tau} K_{eq,rad_{i,p}}(\tau - s + g(0)^{-1}) \mathbf{\Phi}(s)\hat{\mathbf{x}}_p^v ds \\ &- F_{eq,wave_i}(\tau) - \mathbf{\Phi}(\tau)\hat{\mathbf{U}}_i \end{aligned} \tag{42}$$

where $i = 1, .., n_c$, and $M_{eq,tot_{i,p}}$, $B_{eq,visc_{i,p}}$, $G_{eq_{i,p}}$ and $K_{eq,rad_{i,p}}$ are the elements of the matrices $\mathbf{M}_{eq,tot}$, $\mathbf{B}_{eq,visc}$, $\mathbf{G}_{eq}$ and $\mathbf{K}_{eq,rad}$, respectively. PS methods are used to compute the coefficients $\hat{\mathbf{x}}_i^q$, $\hat{\mathbf{x}}_i^v$ and $\hat{\mathbf{u}}_p$ that minimize the residuals (41)-(42) [13]. The PS methods force the residuals of the equations of motion to be zero at a certain number of points in time t_k, called *nodes*. If the number of nodes is $2M + 1$, then a nonlinear system of $2 \times n \times M + 1$ equations is solved.

The optimal control problem defined by the maximization of the cost function (23), subject to the dynamic constraints (21)-(22), is transformed into a finite dimensional optimization problem with cost function (31), and dynamic constraints (41)-(42). Note that, the cost function in (31) is non-convex quadratic and, therefore, a solution to the optimization problem can be locally optimal. In Section V, a convex cost function is proposed, which guarantees that the solution to the optimization problem is a global optimal solution.

V. Convex Cost Function for Receding Horizon Pseudospectral Control

On average, the absorbed power by the PTO and the excitation force power less the dissipated power due to the radiated waves and viscous forces are the same [14]. The maximization of the difference between the excitation force power and the dissipated power yields to an convex optimal control problem in the time domain [5].

Thus, the cost function in (23) can be rewritten as:

$$
\begin{aligned}
J &= \frac{1}{2}\int_{-1}^{1}\Bigg(\mathbf{V}_{eq}^{T}\mathbf{F}_{eq,wave} - \mathbf{V}_{eq}^{T}\mathbf{B}_{eq,visc}\mathbf{V}_{eq} - .. \\
&\quad \mathbf{V}_{eq}^{T}\left(\int_{g(0)^{-1}}^{\tau}\mathbf{K}_{eq,rad}(\tau - s + g(0)^{-1})\mathbf{V}_{eq}d\tau\right)\Bigg)d\tau \\
&= \frac{1}{2}\int_{-1}^{1}\Big(\mathbf{\Phi}(\tau)^{T}\mathbf{X}^{V}\mathbf{X}^{ex,T}\mathbf{\Phi}(\tau) - \mathbf{\Phi}(\tau)^{T}\mathbf{X}^{V}\mathbf{B}_{eq,visc}\mathbf{X}^{V,T}\mathbf{\Phi}(\tau) \\
&\quad - \mathbf{\Phi}(\tau)^{T}\mathbf{X}^{V}\mathbf{X}^{rad,T}\mathbf{\Phi}(\tau)\Big)d\tau \\
&= \frac{1}{2}\mathbf{x}^{ex,T}\mathbf{x} - \frac{1}{2}\mathbf{x}^{T}\tilde{\mathbf{H}}\mathbf{x}
\end{aligned}
\tag{43}
$$

where:

$$\mathbf{X}^{ex} = [\ \hat{\mathbf{x}}_1^{ex}, .., \hat{\mathbf{x}}_{n_c}^{ex}] \tag{44}$$

$$\mathbf{x}^{ex} = [\ \mathbf{0}_{1,N}\ \hat{\mathbf{x}}^{ex,T}\ \mathbf{0}_{1,N}]^{T} \tag{45}$$

$$\mathbf{X}^{rad} = [\ \hat{\mathbf{x}}_1^{rad}, .., \hat{\mathbf{x}}_{n_c}^{rad}] \tag{46}$$

$$\hat{\mathbf{x}}^{rad} = \mathbf{P}_{rad}\hat{\mathbf{x}}^{v} \tag{47}$$

$$\tilde{\mathbf{H}} = \begin{bmatrix} \mathbf{0}_{N,N} & \mathbf{0}_{N,N} & \mathbf{0}_{N,N} \\ \mathbf{0}_{N,N} & \mathbf{P}_{rad} + \mathbf{D}_{visc} & \mathbf{0}_{N,N} \\ \mathbf{0}_{N,N} & \mathbf{0}_{N,N} & \mathbf{0}_{N,N} \end{bmatrix} \tag{48}$$

$$\mathbf{D}_{visc} = \begin{bmatrix} B_{eq,visc_{1,1}}\mathbf{I}_{2M+1} & B_{eq,visc_{1,2}}\mathbf{I}_{2M+1} \\ B_{eq,visc_{2,1}}\mathbf{I}_{2M+1} & B_{eq,visc_{2,2}}\mathbf{I}_{2M+1} \end{bmatrix} \tag{49}$$

with $\mathbf{P}_{rad} \in \mathbb{R}^{N,N}$ is the matrix used to compute the HRCF coefficients of the radiation forces given the HRCF coefficients of the velocities [8]. On the contrary of the cost function in (31), the cost function in (43) is convex and, therefore, the solution to the optimization problem is a global optimal solution.

VI. Results

In [9], the full dynamic model presend in Section II is validated against tank data carried out on a specific three-body hinge-barge device tested in a wave tank using facilities of the U.S. Naval Academy, Annapolis [15]. The dimensions of body 1 are: length$=0.68$ m, width=0.4 m and height=0.1 m. The dimensions of body 2 are: length$=0.28$ m, width=0.4 m and height=0.15m. The dimensions of body 3 are: length$=1$ m, width=0.4 m and height=0.1 m.

A. Monochromatic Waves

The power dissipated by the PTO systems was recorded for a series of regular wave tests performed for a range of frequencies ω from 3.14 rad/sec to 7.54 rad/secs, amplitudes of the waves of 2 cm and direction of the waves along the longitudinal direction of the device. In Figure 2, the full dynamic model shows, in general, a good agreement with the tank data in terms of average absorbed power. Note that, at the frequency $\omega = 7.5$ rad/s, the agreement between the full dynamic model and the tank data is poor. However, the frequency interval over which the energy of the waves is extracted by the WEC is between 3 rad/s and 7 rad/s and, therefore, the frequency $\omega = 7.5$ rad/s is of little interest for this study. Further work is required to improve the accuracy of the full dynamic model, with respect to the tank data, over the entire frequency interval where the tank tests are performed. Furthermore, the peak of the average absorbed power given by the full dynamic model is at a frequency which is slightly greater than the frequency of the peak of the average absorbed power given by the tank data. Additional wave-tank tests with regular waves over the region of maximum power absorption are required to further validate the full dynamic model against the tank data.

In [14], a theory for the calculation of the maximum power absorption of a generic multibody WEC is presented. The theory is formulated in the frequency domain, and it computes the maximum theoretical average power that can be achieved with reactive PTO systems and no constraints on the amplitude of velocities and PTO forces. In Figure 2, the maximum theoretical average power that can be absorbed by a $1/25^{th}$ scale 3-body hinge-barge device at each frequency of the incoming regular wave is shown.

An alternative strategy to PS methods is to consider a linear model in the frequency domain, and compute the optimal damping coefficients of the PTOs that maximizes the energy absorption at each frequency of the incoming wave [14]. In Figure 2, the average power given by the dynamic model with optimal linear damping coefficients for the PTOs is shown.

Next, a passive controller (i.e. only positive power flow *from* the device) based on the reduced model is computed with PS methods, where the torques applied by the PTOs are independent of the relative pitch velocity between the bodies. As Figure 2 shows, the power absorbed with the PS passive control is higher than the power absorbed with a control strategy based on optimal linear damping coefficients. Note that, for the PS passive control, the condition of passivity introduces a non-convex quadratic inequality constraint in the optimization problem given by the cost function (43). Thus, the optimal passive control problem with PS methods can be considered as a nonconvex Quadratically Constrained Quadratic Program (QCQP) [16] and, therefore, a globally optimal solution cannot be guaranteed for the passive control. For the PS passive control, a number of HRCF basis functions $M = 5$ is considered in the approximation of positions, velocities and control forces, as it provides a trade-off between the maximization of the absorbed power and the computational time required to solve the optimization problem.

An *active* controller based on the reduced model is also computed with PS methods, where the flow of power is considered to be bi-directional, so that power from the grid can be injected into the device. The active controller is computed with both non-convex and convex cost function, given in (31) and (43), respectively. As Figure 2, both the PS active controller with convex and nonconvex cost function show similar performances, and compute an absorbed power which is close the maximum theoretical average power. For the PS active control, a number of HRCF basis functions $M = 11$

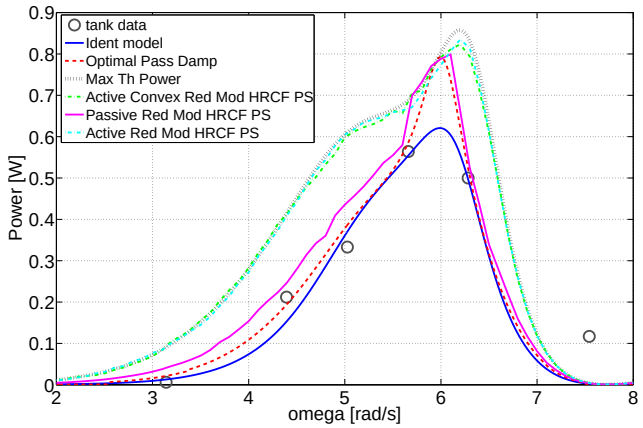

Fig. 2. Comparison between the average power given by the tank data, identified model, max theoretical power, optimal linear damping control, non-convex active reduced model HRCF PS control, convex active reduced model HRCF PS control and passive reduced model HRCF PS control for different frequencies of a regular wave of amplitude $A = 2$ cm.

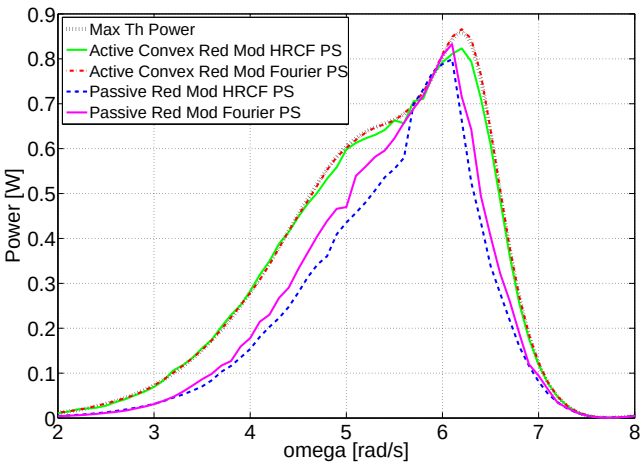

Fig. 3. Comparison between max theoretical power, convex active reduced model Fourier PS control, convex active reduced model HRCF PS control, passive reduced model Fourier PS control and passive reduced model HRCF PS control for different frequencies of a regular wave of amplitude $A = 2$ cm.

is considered in the approximation of positions, velocities and control forces, as it provides an absorbed power which is close to the maximum theoretical average power.

Now, a comparison between PS optimal control with HRCF basis functions and PS optimal control with Fourier basis functions [1] is made. In Figure 3, a comparison between the PS active and passive control with HRCF basis functions, and the PS active and passive control with Fourier basis functions is shown for regular waves. As shown in Figure 3, PS active control with Fourier basis functions computes a slightly greater average absorbed power than the average absorbed power computed with PS active control with HRCF basis functions around the natural resonant frequency of the device. As shown in Figure 3, PS passive control with Fourier basis functions compute a greater average absorbed power than the average absorbed power computed with PS passive control with HRCF basis functions across all the range of frequencies considered. The discrepancy between the average absorbed power computed with the PS passive control with Fourier and HRCF basis functions is due to the nonconvexity of the passive control problem.

B. Polychromatic Waves

For polychromatic waves, under the assumption of the linear superposition of the hydrodynamic loads given by the frequency components of the incoming wave, the maximum theoretical average power is given as:

$$\overline{P}_{th,max} = \sum_{i}^{N_f} \overline{P}_{th,i} A_i^2 \tag{50}$$

where N_f is the number of frequency components of the incoming waves, A_i is the amplitude of the i frequency component and $\overline{P}_{th,i}$ is maximum theoretical average power computed for the i frequency component with unitary amplitude.

In Figure 4, a comparison between the maximum theoretical average power and the average power absorbed with the optimal linear damping control, PS passive control and PS active convex and non-convex control is shown for a polychromatic wave over a simulation time of 100 s. The polychromatic wave is from a JONSWAP spectrum with a significant wave height $H_s = 15\ cm$ and significant period $T = 1.1\ s$. While the PS active and passive control maximize the average absorbed power over the entire time horizon, the coefficients of dash-pot systems of the optimal linear damping control are set equal to their optimal values at the peak frequency of the spectrum of the incoming wave. As shown in Figure 4, the PS active convex and non-convex control compute an average power which asymptotically converges to the maximum theoretical power. Furthermore, as shown in Figure 4, the passive PS control shows better performances than the optimal linear damping control. A number of HRCF basis functions $M = 5$ and $M = 11$ is considered in the approximation of positions, velocities and control forces, for the PS passive and active control, respectively.

In Figure 5, a comparison between the PS active and passive control with HRCF basis functions, and the PS active and passive control with Fourier basis functions is shown for a polychromatic wave over a simulation time of 30 s. The polychromatic wave is from a JONSWAP spectrum with a significant wave height $H_s = 15\ cm$ and significant period $T = 1.1\ s$. As Figure 5 shown, PS active and passive control with HRCF basis functions converge to an average absorbed power which is the same as the average absorbed power computed with PS active and passive control with Fourier basis functions, respectively.

VII. Conclusion

This paper shows the benefits of PS active and passive control with HRCF basis function, with respect to a strategy based

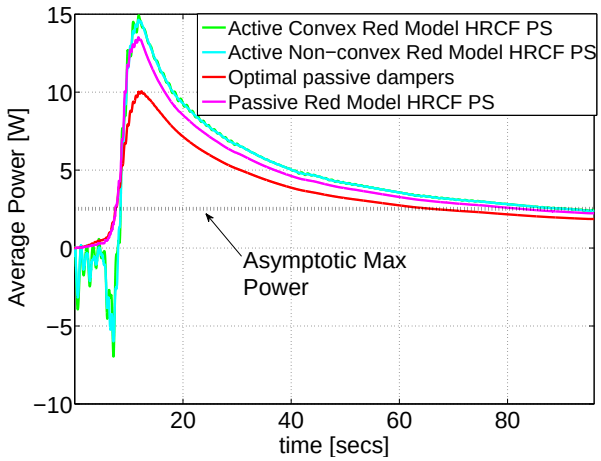

Fig. 4. Comparison between the asymptotic maximum average power and the average power given by the optimal linear damping control, non-convex active reduced model HRCF PS control, convex active reduced model HRCF PS control and passive reduced model HRCF PS control for a polychromatic wave made from a Jonswap spectrum with $H_s = 15$ cm and $T_p = 1.1$ s.

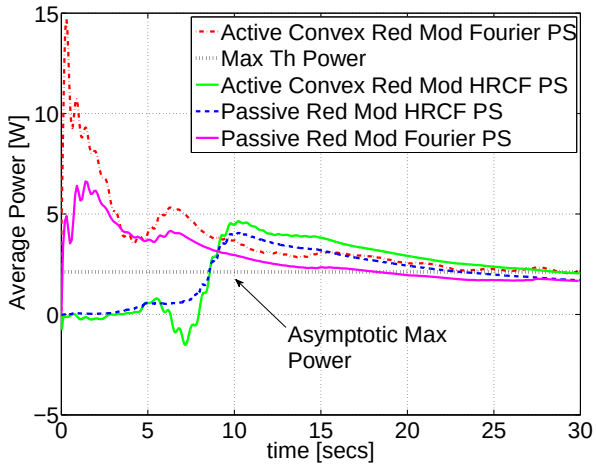

Fig. 5. Comparison between max theoretical power, convex active reduced model Fourier PS control, convex active reduced model HRCF PS control, passive reduced model Fourier PS control and passive reduced model HRCF PS control for a polychromatic wave made from a Jonswap spectrum with $H_s = 15$ cm and $T_p = 1.1$ s.

on optimal linear passive dampers, for the maximization of the energy extracted by a three-body hinge-barge device. In particular, for regular waves, the average absorbed power with PS optimal control with HRCF basis functions is approximately 1.5 times greater than the average absorbed power with optimal linear passive dampers around the resonance of the device. For irregular waves, a similar increase of the average power can be achieved with PS optimal control with HRCF basis functions, with respect to optimal linear dampers. The results also show that the average absorbed power computed by PS passive control is comparable to the average absorbed power computed by PS active control for both regular and irregular waves. However, considering a realistic PTO efficiency [17], a reduction of the benefits of using a reactive control is expected. Also, the costs involved with the use of a bi-directional PTO can exceed the increment in the value of absorbed power that can be achieved with a simpler passive PTO.

The complexity of PS optimal control is greatly reduced by using a reduced equivalent dynamic model, instead of a fully dynamic model, for the description of the dynamics of the device. The reduced equivalent model is described in terms of the relative pitch rotations only, which are the modes that are used to extract energy from the device. A convex optimization problem for the active control with the reduced equivalent model can be found, which guarantees a globally optimal solution. However, with the reduced equivalent model, no constraints on the heave and absolute pitch rotation of the central barge can be enforced, as the reduced equivalent model is described in terms of the relative pitch rotations only.

In terms of basis functions used for the PS methods, while HRCF basis functions represent both the transient and steady-state response of the device, Fourier basis functions can only represents steady-state response of the device. Therefore, PS methods based on HRCF basis functions, rather than PS methods based Fourier basis functions, are well suited for the implementation the real-time control of the WEC. In terms of power absorption performance, for regular waves, PS active control with Fourier basis functions computes a slightly greater average absorbed power than the average absorbed power computed with PS active control with HRCF basis functions, around the natural resonant frequency of the device. For regular waves, PS passive control with Fourier basis functions compute a greater average absorbed power than the average absorbed power computed with PS passive control with HRCF basis functions across all the range of frequencies considered. The discrepancy between the average absorbed power computed with the PS passive control with Fourier and HRCF basis functions is due to the nonconvexity of the passive control problem. For irregular waves, PS active and passive control with HRCF basis functions converge to an average absorbed power which is the same as the average absorbed power computed with PS active and passive control with Fourier basis functions.

ACKNOWLEDGMENT

This paper is based upon work supported by Science Foundation Ireland under Grant No. 12/RC/2302 for the Marine Renewable Ireland (MaREI) centre.

REFERENCES

[1] Paparella, F. and Ringwood, J.V., "Optimal control of a three-body hinge-barge wave energy device using pseudo-spectral methods," *IEEE Transactions on Sustainable Energy*, vol. 8, no. 1, pp. 200 – 207, 2017.
[2] Canuto, C., Hussaini, Y., Quarteroni, A., and Zang, T., *Spectral Methods: Fundamentals in Single Domains*. Springer, 2006.
[3] Fornberg, B., *A Practical Guide to Pseudospectral Methods*. Cambridge University Press, 1996.
[4] Bacelli, G. and Ringwood, J.V., "Numerical optimal control of wave energy converters," *IEEE Transactions on Sustainable Energy*, vol. 6, no. 2, pp. 294–302, 2015.

[5] Hals, J., Falnes, J., and Moan, T., "Constrained optimal control of a heaving buoy wave-energy converter," *J. Offshore Mech. Arct. Eng.*, vol. 133, pp. 0 114 011–01 140 115, 2011.
[6] Faedo,N., Olaya,S., and Ringwood, J. V., "Optimal control, MPC and MPC-Like algorithms for wave energy systems: An overview," *IFAC Journal of Systems and Control*, Under review.
[7] D. Huybrechs, "On the Fourier extension of nonperiodic functions," *SIAM J. Numer. Anal.,*, vol. 47, no. 6, pp. 4326–4355, 2010.
[8] Genest, R. and Ringwood, J.V., "Receding horizon pseudospectral control for energy maximisation with application to wave energy devices," *IEEE Transactions on Control System Technology*, vol. 25, no. 1, pp. 29 – 38, 2016.
[9] Paparella, F., Bacelli, G., Paulmeno, A., Mouring, S. E., and Ringwood, J.V., "Multi-body modelling of wave energy converters using pseudospectral methods with application to a three-body hinge-barge device," *IEEE Transactions on Sustainable Energy*, vol. 7, no. 3, pp. 966 – 974, 2016.
[10] Babarit, A., "Optimisation hydrodynamique et controle optimal dun recuperateur de lenergie des vagues," Ph.D. dissertation, École centrale de Nantes, 2005.
[11] Olaya, S., Bourgeot, J. M., and Benbouzid, M., "Optimal control for a self-reacting point absorber: A one-body equivalent model approach," in *Proc. of Power Electronics and Application Conference and Exposition (PEAC)*, 2014.
[12] Orel, B. and Perne, A., "Computations with Half-Range Chebyshev polynomials," *J. Comput. Appl. Math.*, vol. 236, no. 7, pp. 1753–1765, 2012.
[13] Elnagar, G., Kazemi, M. A., and Razzaghi, M., "The pseudospectral Legendre method for discretizing optimal control problems," *IEEE Transactions on Automatic Control*, vol. 40, no. 10, 1995.
[14] J. Falnes, *Ocean Waves and Oscillating Systems*. Cambridge, U.K.: Cambridge University Press, 2002.
[15] Paulmeno, A., "An Experimental Analysis of the Optimal Design Conditions for a Model Scale McCabe Wave Pump," Department of Naval Architecture and Ocean Engineering, United States Naval Academy Annapolis, Maryland 21402, Independent Research in Ocean Engineering Honors Final Report, May 2013.
[16] Boyd, S. and Vandenberghe, L., *Convex Optimization*. Cambridge University Press, 2004.
[17] Genest, R., Bonnefoy, F., Clément, A. H., and Babarit, A., "Effect of non-ideal power take-off on the energy absorption of a reactively controlled one degree of freedom wave energy converter," *Applied Ocean Research*, vol. 48, pp. 236–243, 2014.